Solvent Effects on the Resonance Raman and Hyper-Raman Spectra and First Hyperpolarizability of *N*,*N*-Dipropyl-*p*-nitroaniline

Lian C. T. Shoute,[†] Robin Helburn,[‡] and Anne Myers Kelley*[,†]

School of Natural Sciences, University of California, Merced, P.O. Box 2039, Merced, California 95344, and Department of Chemistry and Physical Sciences, Pace University, 1 Pace Plaza, New York, New York 10038

Received: October 7, 2006; In Final Form: December 8, 2006

Linear absorption spectra, resonance Raman spectra and excitation profiles, and two-photon-resonant hyper-Rayleigh and hyper-Raman scattering hyperpolarizability profiles are reported for the push−pull chromophore *N*,*N*-dipropyl-*p*-nitroaniline in seven solvents spanning a wide range of polarities. The absorption spectral maximum red shifts by about 2700 cm^{-1}, and the symmetric $-NO_2$ stretch shifts to lower frequencies by about 11 cm^{-1} from hexane to acetonitrile, indicative of significant solvent effects on both the ground and excited electronic states. The intensity patterns in the resonance Raman and hyper-Raman spectra are similar and show only a small solvent dependence except in acetonitrile, where both the Raman and hyper-Raman intensities are considerably reduced. Quantitative modeling of all four spectroscopic observables in all seven solvents reveals that the origin of this effect is an increased solvent-induced homogeneous broadening in acetonitrile. The linear absorption oscillator strength is nearly solvent-independent, and the peak resonant hyperpolarizability, $\beta(-2\omega;\omega,\omega)$, varies by only about 15% across the wide range of solvents examined. These results suggest that the resonant two-photon absorption cross sections in this chromophore should exhibit only a weak solvent dependence.

Introduction

Solvent effects on the linear electronic spectra (absorption and fluorescence) of organic molecules have been a topic of experimental and theoretical investigation for more than 50 years.[1−9] Solvent effects on the relative energies of different electronic states lead to shifts in absorption and emission frequencies. These are comparatively easy to measure and can often be understood in terms of the electrostatic and dispersive interactions between the charge distributions in the molecule's electronic states and the bulk polarity and polarizability of the solvent. Solvent effects on the intensities of allowed electronic transitions (absorption oscillator strengths or fluorescence radiative rates) tend to be smaller and more variable from one molecule to another. The bandshapes of electronic spectra (linewidths and vibronic structure) may also be significantly solvent dependent, and while these effects are often clearly observable in the absorption spectrum, they can be better understood by analyzing coupled absorption and emission spectra (static and dynamic Stokes shifts)[10,11] and/or electronically resonant Raman spectra.[12−17]

Nonlinear spectra such as two- and three-photon absorption and other electronically resonant multiphoton processes are also subject to solvent effects, but these have been less well studied. The frequencies and bandshapes of multiphoton absorption spectra should be determined by the same factors that influence one-photon spectra, although strongly two-photon-allowed states, in particular, often have very different structures and charge distributions from one-photon states and may experience very different interactions with any given solvent. The cross sections for multiphoton absorption might be expected to exhibit complex solvent dependences because such processes typically involve multiple paths through different intermediate (virtual) states that are differently influenced by solvent. Indeed, a few published studies of two-photon absorption cross sections report rather strong solvent dependences that are not straightforward to explain.[18,19] There have also been some theoretical studies of solvent effects on two-photon absorption cross sections,[20−29] and recent work using time-dependent density functional theory (DFT) methods with continuum solvation models has demonstrated encouraging progress.[20]

Molecular first hyperpolarizabilities (β) are often measured through incoherent second harmonic (hyper-Rayleigh) scattering. The solvent dependence of the electronically nonresonant β has been the subject of a number of experimental and computational studies.[30−37] When the excitation falls within an electronic two-photon resonance, the hyper-Rayleigh and hyper-Raman scattering are greatly enhanced and their intensities become dependent upon the vibronic structure and transition linewidths of the resonant electronic state and also to its one- and two-photon oscillator strengths. These are analogous considerations to those that influence the intensity of linear resonance Raman scattering. Solvent effects on resonance Raman intensities have been studied in considerable detail,[38−44] but there has been very little work on the corresponding resonant nonlinear processes.

Recently we reported initial efforts to measure and model the solvent-dependent two-photon resonant hyper-Rayleigh and hyper-Raman hyperpolarizability profiles, as well as the linear absorption spectra and resonance Raman cross section profiles, for the nonlinear optical chromophore *N*,*N*-dimethylaminonitrostilbene (DANS) and a water-soluble analog.[45] The observed solvent effects were rather small compared with the uncertainties in the data but did indicate that the peak resonant hyperpolarizabilities increase as the absorption maximum red shifts. In comparison to similar push−pull molecules such as *p*-nitroa-

* To whom correspondence should be addressed.
[†] University of California, Merced.
[‡] Pace University.

10.1021/jp066599s CCC: $37.00
Published on Web 01/26/2007

niline (PNA), DANS exhibits comparatively weak solvent effects on its *linear* absorption spectra. In this paper we report a corresponding study on *N*,*N*-dipropyl-*p*-nitroaniline (DPPNA), which exhibits fairly strong absorption solvatochromism similar to that of the parent PNA but absorbs at longer wavelengths.[46] The linear and nonlinear optical properties of the parent PNA and its *N*,*N*-dimethyl derivative have been widely studied[31,33,35,47−58] and provide a point of reference for our work on DPPNA.

Direct two-photon absorption or two-photon excited fluorescence excitation spectra of large molecules in solution are typically unstructured and provide little information beyond the approximate state energy and two-photon cross section for the resonant two-photon state. Multiple electronic transitions are usually difficult to discern in these broad absorption spectra. Resonance hyper-Raman spectra provide a wealth of vibrational detail about the changes in molecular geometry induced by electronic excitation, and changes in the intensity patterns as the excitation wavelength is tuned can reveal the presence of overlapping states.[59] Changes in solvent are expected to appear in the hyper-Raman intensities through solvent effects on the two-photon cross sections and/or excited-state geometries of a single resonant state, as well as through changes in the quantum mechanical interferences among multiple contributing states that undergo different solvent shifts. These factors make resonance hyper-Raman a rich source of information about solvent effects on one- and two-photon electronic states but also complicated to interpret unambiguously.

Experimental Methods

DPPNA was synthesized as described previously.[58] The solvents hexane (Fisher, HPLC), cyclohexane (Aldrich, HPLC), 1,4-dioxane (ACROS, spectroscopic), ethyl acetate (ACROS, spectroscopic), dichloromethane (Sigma-Aldrich, spectroscopic), acetone (Fisher, HPLC), and acetonitrile (Fisher, HPLC) were used as received. The spectroscopic measurements were carried out using the methods and instrumentation described in previous publications.[45,60,61] DPPNA concentrations were 0.04−0.05 mM for the hyper-Rayleigh intensity measurements, 0.3−0.5 mM for the hyper-Raman, and 0.07−0.5 mM for the resonance Raman. DPPNA has good solubility in all of the solvents used, and the absorption spectra in all seven solvents show no concentration dependence between 1 and 4 mM. Hyper-Raman and hyper-Rayleigh hyperpolarizabilities were determined relative to the hyper-Rayleigh scattering of acetonitrile as an external standard.[60] Resonance Raman cross sections were determined relative to the Raman cross sections of the following solvent lines as internal standards: hexane 1452 cm^{-1}, cyclohexane 1026 cm^{-1}, dioxane 1013 cm^{-1}, ethyl acetate 633 cm^{-1}, dichloromethane 702/740 cm^{-1}, acetone 787 cm^{-1}, and acetonitrile 919 cm^{-1}. The solvent cross sections have either been published[52] or were determined relative to those reported previously as internal or external standards (measured at ten excitation wavelengths between 362 and 515 nm and fit to an A-term dependence).

In both the linear and nonlinear experiments, the relative intensities of the DPPNA and standard Raman lines were examined as a function of laser power to check for photochemistry or depletion of the ground-state population. In the less polar solvents, particularly hexane and cyclohexane, the resonance Raman intensities exhibited a strong laser power dependence probably attributable to formation of relatively long-lived triplet states in high yield. The room-temperature triplet state lifetime of the *N*,*N*-dimethyl analog exceeds 1 μs in both benzene and dioxane.[62] Obtaining power-independent solute to solvent Raman intensity ratios required reducing the laser power to below 5 μW, at which point the signal-to-noise ratio was fairly low for all but the one or two strongest DPPNA lines. However, the *relative* DPPNA intensities showed no power dependence up to 2 mW (i.e., no new lines assignable to the triplet were observed). Therefore, the relative intensities of the lines in the DPPNA resonance Raman spectra were first obtained from spectra taken at higher powers (20 μW) exhibiting a high signal-to-noise ratio, and the absolute cross sections for the strongest one or two lines were then determined from spectra at the lowest laser powers. No significant laser power dependence of the DPPNA hyper-Raman to acetonitrile hyper-Rayleigh intensity ratio was observed at incident laser powers below 100 mW.

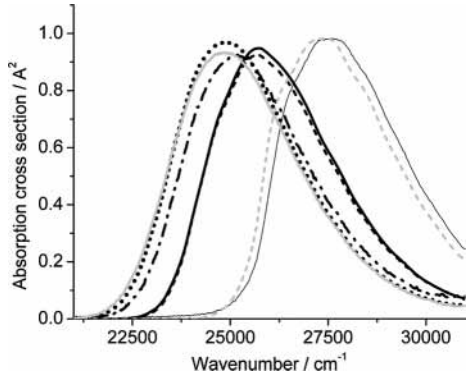

Figure 1. Absorption spectra of DPPNA in hexane (thin black), cyclohexane (gray dashes), ethyl acetate (thick black), dioxane (black dashes), acetone (dot-dashed), dichloromethane (dots), and acetonitrile (thick gray).

Computational Methods

The linear absorption spectra and the resonance Raman, hyper-Rayleigh, and hyper-Raman excitation profiles were numerically simulated with a common model for the ground and excited electronic states as described in previous publications.[45,59,60] We assumed a single resonant electronic state, equal ground- and excited-state vibrational frequencies, and no dependence of the electronic transition moment on vibrational coordinates, the same assumptions employed in our earlier resonance Raman excitation profile analysis of *p*-nitroaniline.[52] The vibrational hyperpolarizability contribution to the hyper-Rayleigh and hyper-Raman intensities, which scales as the derivative of the ground-state permanent dipole moment with respect to vibrational coordinate (e.g., the ground-state vibrational infrared intensity), was included as described in previous publications.[45,59] Because of complexities in calculating hyper-Raman combination bands and overtones when the vibrational paths are included, the combination band and overtone intensities were modeled only in the resonance Raman.

DFT calculations of the ground-state geometry and vibrational frequencies were carried out with the B3LYP density functional and the 6-311G** basis as implemented in Gaussian 03.[63] Calculations of the electronic transition energies were performed with the ZINDO method and using time-dependent DFT, also as implemented in Gaussian 03, at the optimized ground-state DFT geometry.

Results

Figure 1 shows the linear absorption spectra of DPPNA in all seven solvents used. The absorption maximum red shifts by about 2700 cm^{-1} from hexane to acetonitrile. There is also a

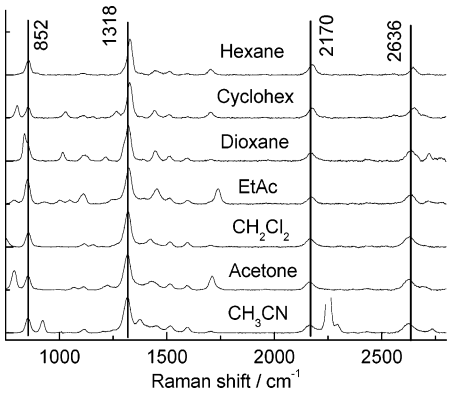

Figure 2. Resonance Raman spectra of DPPNA in seven solvents. Excitation is at 368−375 nm (26670−27170 cm^{-1}), and concentrations are 0.35−0.46 mM. The vertical lines at the labeled Raman shifts indicate the four strongest lines in the spectrum: two fundamentals, a combination band, and an overtone. Most of the other strong peaks in the spectra are solvent lines.

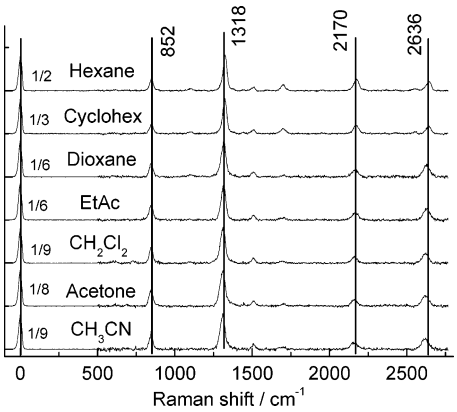

Figure 3. Resonance hyper-Raman spectra of DPPNA in seven solvents. Excitation is at 744 nm (two-photon energy 26880 cm^{-1}), and concentrations are 0.35−0.46 mM. The vertical lines at the labeled Raman shifts indicate the five strongest lines in the spectrum: hyper-Rayleigh, two hyper-Raman fundamentals, a combination band, and an overtone. The hyper-Rayleigh peaks are scaled as indicated. No solvent hyper-Raman lines are evident in these spectra.

hint of vibronic structure in the nonpolar solvents, hexane and cyclohexane.

Representative resonance Raman and resonance hyper-Raman spectra in all seven solvents are shown in Figures 2 and 3. The excitation wavelengths (two-photon wavelength for the hyper-Raman) fall on the blue side of the absorption in the more polar solvents, and on the red side in cyclohexane and hexane. The Raman and hyper-Raman spectra are dominated by the symmetric NO_2 stretch near 1318 cm^{-1}, the NO_2 scissors mode near 852 cm^{-1}, and relatively strong overtones and combination bands of these two modes. There are also weaker fundamentals at about 1112 cm^{-1} (phenyl-NO_2 stretch), 1513 cm^{-1} (ring-N_{amino} stretch and ring H rock), and 1596 cm^{-1} (phenyl mode 8a, quinoidal stretch). The main hyper-Raman bands are quite strong compared with the hyper-Rayleigh, within a factor of 5 in integrated areas at this excitation wavelength, and the strongest overtones and combination bands are only two to three times weaker than the strongest fundamental. This is characteristic of a molecule in which ground- to excited-state geometry change is fairly large and is localized in just a few vibrational modes. The intensity patterns in both Raman and hyper-Raman spectra are qualitatively similar in all solvents spanning a wide range of polarities.

The symmetric NO_2 stretch shifts from about 1327 cm^{-1} in hexane and cyclohexane to 1316 cm^{-1} in acetone and acetonitrile, indicative of a solvent polarity effect on the ground-state structure. Similar effects in the *N*,*N*-dimethyl analog (DMPNA) were studied in detail by Fujisawa and co-workers.[56] With nonresonant excitation (488 nm), they observed a solvent polarity dependent shift of this mode from ∼1329 cm^{-1} in hexane to ∼1312 cm^{-1} in acetonitrile (and 1300 cm^{-1} in water), consistent with our observations. They also reported that the frequency of this mode in DMPNA varied by 7−8 cm^{-1} in acetonitrile and by about 15 cm^{-1} in water as the excitation was tuned through the absorption band, and attributed this to selective excitation of different members of an inhomogeneously solvated ensemble. In contrast, for DPPNA in all solvents examined we find that the frequency of this mode is independent of excitation wavelength to within our experimental uncertainty of ∼2 cm^{-1}.

In previous publications[45,59] we showed that the "vibrational" paths, those in which a vibrationally excited level of the ground electronic state serves as the intermediate state in the two-photon transition, can make an important contribution to the hyper-Raman scattering of modes that are strongly infrared active. The ground-state IR intensities, in absolute units, determine the dipole moment derivatives required to evaluate these terms. We were not able to obtain the IR absorbances for this molecule, and previous experience with molecules of this type indicated that the DFT calculations are not very good quantitative predictors of IR intensities.[45,59,64] However, all of the strong Raman modes of DPPNA have similar frequencies and normal mode descriptions to vibrations observed in DANS, for which experimental IR intensities are available.[65] Therefore, we set the IR intensities for the 1112, 1318, 1513, and 1596 cm^{-1} vibrations of DPPNA equal to the experimental values for the corresponding modes of DANS.[45,65] The IR intensity of the DANS mode corresponding to the 852-cm^{-1} line of DPPNA is not available, but as our DFT calculations predict it to be weak, we set it to zero in the simulations. Table 1 summarizes the experimental and calculated vibrational frequencies, normal mode descriptions, and ground-state dipole moment derivatives for the five strongly Raman-active modes of DPPNA.

The experimental profiles were then simulated to find the parameters that best reproduce all of the spectroscopic data. The data modeled were the absorption spectrum, eight resonance Raman excitation profiles (the five fundamentals, the 852 + 1318 combination band, and the 852 and 1318 overtones), the hyper-Rayleigh hyperpolarizability profile, and two hyper-Raman profiles (the 852 and 1318 fundamentals). Figures 4−6 show representative fits in solvents of high (acetonitrile), moderate (ethyl acetate), and low (hexane) polarity. Table 2 gives the fitting parameters in all seven solvents.

With regard to the linear spectra (absorption and resonance Raman), the principal difference between acetonitrile and ethyl acetate is the substantial red-shift of both the absorption spectrum and the excitation profiles in the more polar solvent, appearing as a 1800-cm^{-1} shift in the electronic zero−zero energy in the fitting parameters of Table 2. The resonance Raman intensities of all modes are also reduced in the more polar solvent, as manifested by the nearly factor of 2 difference in the electronic homogeneous line width. In the nonpolar solvents, hexane and cyclohexane, the spectra further blue shift. The best-fit homogeneous linewidths are not much different in hexane and cyclohexane than in the solvents of moderate polarity, although the inhomogeneous widths (a parameter that is not very well defined in the fitting process) are slightly

TABLE 1: Five Most Strongly Raman-Active Modes of DPPNA

exptl freq	calcd freq[a]	calcd mode[a]	calcd IR intensity[b] (km mol^{-1}); calcd dμ/dq (e**Å**)	dμ/dq (e**Å**) from DANS[c]
1596	1644	8a (quinoidal ring stretch)	364; 0.088	0.064
1513	1438	phenyl-N_{amino} str, ring H rock	33; 0.028	0.022
1318	1362	sym NO_2 str	862; 0.148	0.136
1112	1132	phenyl-NO_2 str	208; 0.080	0.040
852	870	NO_2 sciss, ring mode 1	14; 0.024	

[a] B3LYP/6-311g** DFT calculation. [b] B3LYP/6-311 g** DFT values converted from km mol^{-1} to eÅ as described in ref 59. [c] Values used in ref 45 (see text).

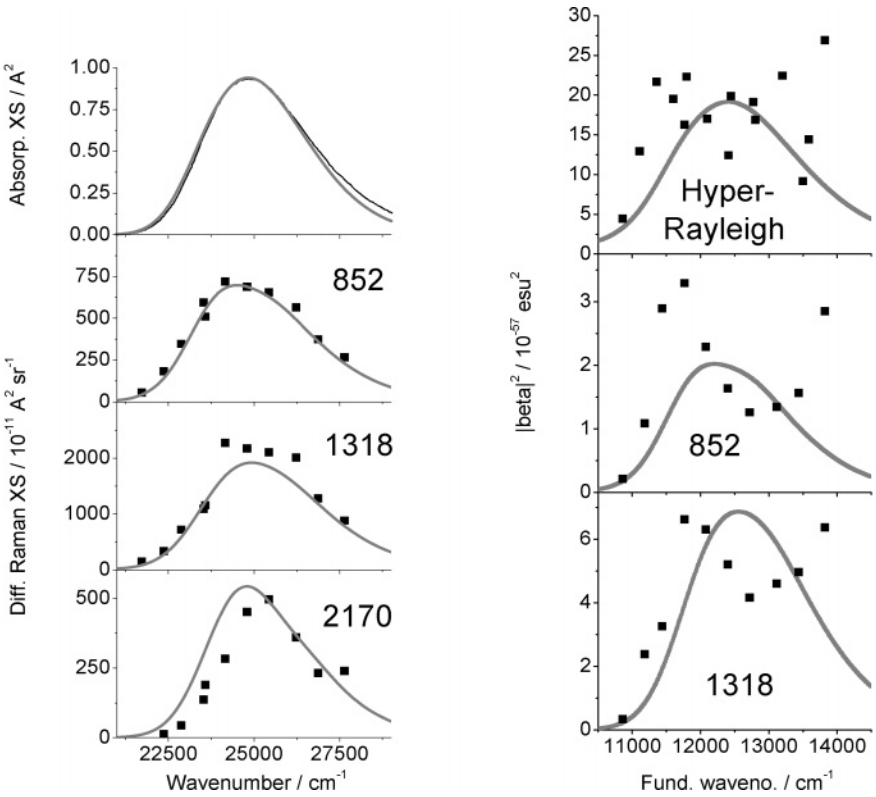

Figure 4. Left: Experimental (thin black line and points) and calculated (thick gray lines) absorption spectrum and Raman excitation profiles for two fundamentals and a combination band, for DPPNA in acetonitrile. Right: Hyper-Rayleigh and hyper-Raman profiles.

reduced. Also, while the best-fit excited-state geometry changes are quite similar in all seven solvents, Δ for the 1318 cm^{-1} mode is slightly larger in cyclohexane and hexane than in any of the polar solvents, while Δ for the 852 cm^{-1} mode is smaller in the nonpolar solvents.

The hyperpolarizability profiles also red shift with increasing solvent polarity, roughly tracking the linear absorption spectra. The hyper-Raman intensities, like the resonance Raman, are considerably lower in acetonitrile than in any of the other solvents, although the uncertainties in the experimental points are rather large. The hyper-Rayleigh and hyper-Raman intensities depend on all of the same parameters as do the absorption and resonance Raman profiles, plus the difference between excited- and ground-state permanent dipole moments ($\Delta\mu$). This quantity is found to be quite similar for all seven solvents, decreasing slightly with increasing solvent polarity. The hyper-Raman profiles in acetonitrile are poorly fit by the simulations, exhibiting local minima near the calculated maxima. We were unable to reproduce this behavior without assuming more than one contributing resonant electronic state, for which there is little or no other support (see Discussion).

Discussion

ZINDO electronic structure calculations (in vacuo) at the ground-state DFT geometry predict that the predominantly highest-occupied molecular orbital → lowest-unoccupied molecular orbital excitation is well isolated from other one-photon-allowed low-lying transitions. Two other transitions with 6−8-fold lower oscillator strengths are predicted to lie about 11 000 cm^{-1} higher. Time-dependent DFT calculations predict that the two lowest-energy significantly one-photon-allowed transitions are separated by more than 16 000 cm^{-1}. Although solvation may shift the state energies considerably and cause some changes in oscillator strength, these calculations strongly suggest that a single electronic transition is responsible for most of the absorption band shown in Figure 1 and that modeling these spectra with a single resonant electronic state is reasonable. There is little evidence that multiple electronic states can explain the poor fits to the hyper-Raman profiles in acetonitrile. Note that states that are *only* two-photon allowed can contribute to the hyper-Raman intensity only through the B-term mechanism,[68] which is expected to be considerably weaker than the A-term that governs scattering from states that are both one- and two-photon allowed. Our DFT calculations using the B3LYP density functional, as well as semiempirical AM1 calculations, produce a structure that is nearly planar (apart from the propyl groups). These results are consistent with the crystal structure in which the nitro and dialkylamino groups of DPPNA exhibit only slight ($\leq 5°$) deviations from planarity with the

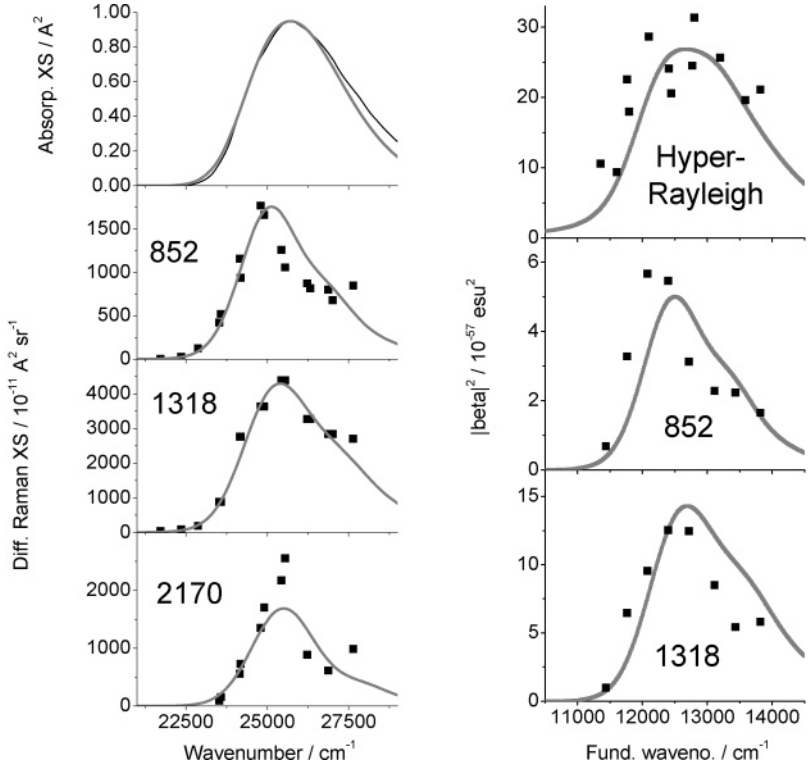

Figure 5. Left: Experimental (thin black line and points) and calculated (thick gray lines) absorption spectrum (top) and Raman excitation profiles for two fundamentals and a combination band, for DPPNA in ethyl acetate. Right: Hyper-Rayleigh and hyper-Raman profiles.

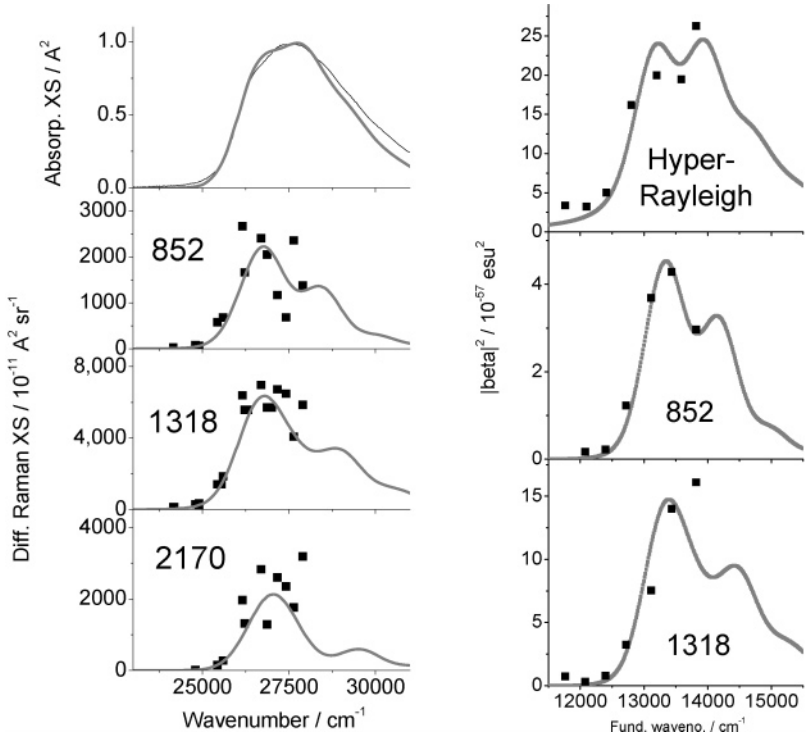

Figure 6. Left: Experimental (thin black line and points) and calculated (thick gray lines) absorption spectrum (top) and Raman excitation profiles for two fundamentals and a combination band for DPPNA in hexane. Right: Hyper-Rayleigh and hyper-Raman profiles.

phenyl ring,[58] although it is possible that the solution-phase structures are more nonplanar.

Figure 7 plots the peak resonance Raman and resonance hyper-Raman intensities for the strongest Raman line, the 1318-cm^{-1} NO_2 stretch, as a function of the solvent ET(30) parameter,[67] a measure of solvent polarity that distributes the seven solvents conveniently along the *x* axis. These values are averages of the three (in some cases two) highest intensities on the Raman or hyper-Raman excitation profiles, with their associated error bars. The Raman cross sections have been divided by the frequency prefactor $\omega^3_{scatt}\omega_{laser}$ to make them proportional to the Raman polarizabilities for proper comparison with the hyper-Raman hyperpolarizabilities. In both spectroscopies the intensities are significantly lower in acetonitrile than in any of the other solvents, and slightly higher in hexane and cyclohexane than in the polar solvents. There is a good

TABLE 2: Spectral Simulation Parameters[a]

	CH_3CN	CH_2Cl_2	acetone	dioxane	ethyl acetate	cyclohexane	hexane
ET(30)[b]	45.6	40.7	42.2	36.0	38.1	30.9	31.0
E_0/cm^{-1}	22700	23500	23900	24500	24500	26000	26300
μ/eÅ	1.43	1.46	1.40	1.36	1.41	1.38	1.38
Γ/cm^{-1}	1600	1000	900	850	900	900	800
θ/cm^{-1}	600	700	750	650	750	500	500
$\Delta\mu$/eÅ	0.90	0.95	0.95	0.95	1.0	1.0	1.05
Δ (852 cm^{-1})	0.97	0.83	0.82	0.80	0.82	0.70	0.70
Δ (1112 cm^{-1})	0.30	0.25	0.24	0.30	0.24	0.27	0.32
Δ (1318 cm^{-1})	1.10	1.15	1.12	1.12	1.12	1.18	1.20
Δ (1513 cm^{-1})	0.27	0.28	0.25	0.23	0.30	0.34	0.38
Δ (1596 cm^{-1})	0.23	0.21	0.18	0.22	0.17	0.25	0.25

[a] Definitions: E_0, electronic zero−zero transition energy; μ, ground- → excited-state transition length; Γ, electronic homogeneous line width, modeled as a single overdamped Brownian oscillator;[13,66] θ, electronic inhomogeneous broadening (Gaussian) standard deviation; $\Delta\mu$, difference between excited and ground state permanent dipole moments; Δ, difference between excited- and ground-state equilibrium geometries along each normal mode, in dimensionless normal coordinates. Common to all solvents: ground-state ($\partial\mu/\partial$q) values from Table 1. [b] Reference 67.

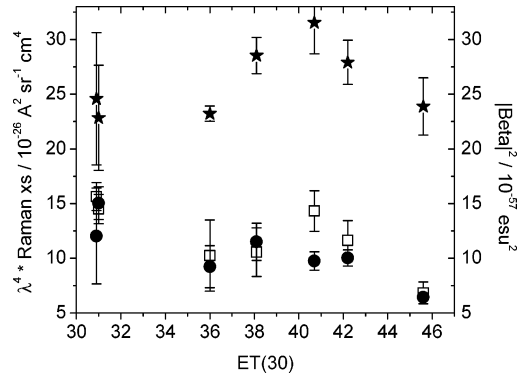

Figure 7. Peak resonance Raman cross section divided by frequency prefactor (open squares) and peak hyper-Raman hyperpolarizability squared (solid circles) for the 1318-cm^{-1} line of DPPNA as a function of solvent ET(30) parameter. Peak hyper-Rayleigh hyperpolarizability squared is also shown (stars).

correlation between the solvent dependences of the Raman and hyper-Raman scattering intensities. It should be noted that the two experiments use completely different methods for converting spectra to absolute intensities by reference to internal or external standards, so any systematic errors in making these conversions should be uncorrelated.

A strong correlation between resonance Raman and resonance hyper-Raman intensities is expected if the two-photon absorption cross sections are approximately independent of solvent as are the linear absorption cross sections (see Figure 1). The factors that determine the resonance Raman or resonance hyper-Raman cross sections, in the fully electronically allowed (A-term) limit, can be divided into three groups: the geometry changes between ground and excited states (normal mode Δs), the electronic transition strengths (one-photon up and one-photon down for resonance Raman, two-photon up and one-photon down for hyper-Raman), and the dephasing rate for the resonant electronic state. In the limit of a single resonant electronic state, the geometry changes between ground and excited states influence the Raman and hyper-Raman intensities in the same way;[69,70] if the Δ values vary with solvent, they should lead to the same solvent dependence of the intensities for both linear Raman and hyper-Raman scattering. Similarly, the dephasing rate of the resonant electronic state affects the linear and nonlinear Raman intensities in the same way.[69,70] In the single resonant state limit, the product of two-photon and one-photon oscillator strengths goes as the square of the one-photon transition dipole, the same quantity that appears in the resonance Raman intensity, multiplied by the permanent dipole moment difference, $\Delta\mu$. Therefore, any difference between the solvent dependences of the linear and nonlinear Raman intensities would have to arise from the solvent dependence of $\Delta\mu$. While simple "two-state, two-form" models for the first hyperpolarizability do predict that $\Delta\mu$ should decrease with increasing solvent polarity,[71−73] for many push−pull molecules including the parent PNA[52] this appears to be a small effect as implied by the fitting parameters of Table 2.

Thus, while both the linear resonance Raman and the resonance hyper-Raman intensities vary with solvent, they both do so in about the same way. There appear to be two principal sources for this solvent dependence. The increased electronic homogeneous line width in acetonitrile compared with all other solvents (Table 2) causes the intensities in this solvent to be lower. Rapid electronic dephasing in acetonitrile has been observed in previous resonance Raman studies of push−pull molecules[16,17,64] and may be attributed to the combination of a large solvent dipole and a particularly large and rapid inertial component to the solvent reorganization dynamics.[74] A solvent isotope effect has also been reported for the resonance Raman intensities of betaine-30 in CH_3CN and CD_3CN.[75] The origin of the slightly increased Raman and hyper-Raman intensities in hexane and cyclohexane is harder to assign, but it appears to arise from a combination of the increased $\Delta_{1318}/\Delta_{852}$ ratio (which transfers intensity from the 852-cm^{-1} line into the already strong 1318-cm^{-1} line) and the slightly reduced total electronic line width (homogeneous plus inhomogeneous), which tends to make the excitation profiles more sharply peaked.

Figure 7 also plots the peak hyper-Rayleigh hyperpolarizability, $|\beta(-2\omega;\omega,\omega)|$,^{2} as a function of solvent ET(30). This quantity does not track well with the Raman and hyper-Raman intensities and it appears to have a weak maximum at intermediate solvent polarities, although the data are not sufficiently robust to warrant such a conclusion. The peak $|\beta|^2$, the quantity proportional to the hyper-Rayleigh scattering intensity, varies by less than 30% across the range of solvents used, and the hyperpolarizability itself, the quantity usually reported in studies of the nonlinear optical properties of chromophores, varies by less than 15%. For comparison, the nonresonant first hyperpolarizability measured across a wide range of solvent polarities is reported to vary by nearly a factor of 2 for *N*,*N*-dimethyl PNA and by about 40% for PNA.[31] Variations of comparable magnitude persist for PNA even when the two-state model for the hyperpolarizability is used to extrapolate the measured values to zero frequency.[35,49] We also found a somewhat stronger solvent dependence of the resonant hyperpolarizability in DANS even though our measurements in that molecule spanned a smaller range of solvent polarities.[45] In DANS we were unable to model the hyper-Rayleigh intensities with the same param-

eters that fit all of the other spectroscopic observables and suggested that this might be attributed to nonresonant contributions to the scattering, which should be more important for hyper-Rayleigh than for hyper-Raman. No such discrepancy is observed for DPPNA, where the parameters that best fit the linear absorption, resonance Raman, and hyper-Raman profiles also give reasonable fits to the hyper-Rayleigh profiles.

It has long been known that measurements of resonance Raman cross sections allow, in principle, separation of the homogeneous and inhomogeneous contributions to the total electronic spectral breadth.[12] Increasing the homogeneous width reduces the Raman cross sections both at the peak of the electronic resonance and integrated over the excitation profile. In contrast, the absorption spectrum is broadened with no change in its integrated area. The homogeneous width is only one contribution to the total electronic spectral breadth, which is often dominated by inhomogeneous broadening and/or vibronic structure, and the linear absorption spectrum of DPPNA (Figure 1) is not notably broader in acetonitrile than in the other polar solvents. These same statements apply to two-photon absorption and scattering in the absence of any intermediate one-photon resonance. Our results suggest that DPPNA should exhibit only a slight solvent effect on its two-photon absorptivity because the factors that contribute to the two-photon oscillator strength are nearly independent of solvent. This prediction contrasts with recent experimental observations of strongly solvent dependent two-photon absorption in other chromophores.[18,19] As DPPNA is not very fluorescent (this is part of the reason it was chosen for these Raman and hyper-Raman experiments), its two-photon absorptivity would have to be measured by a direct technique such as z-scan. To our knowledge no two-photon absorption measurements have been reported even for the parent PNA, but they would provide a useful check on the predictions of our nonlinear scattering experiments.

Acknowledgment. This work was supported by National Science Foundation Grant CHE-0342816 to A.M.K.

References and Notes

(1) Wong, M. W.; Frisch, M. J.; Wiberg, K. B. *J. Am. Chem. Soc.* **1991**, *113*, 4776.
(2) Myers, A. B.; Birge, R. R. *J. Chem. Phys.* **1980**, *73*, 5314.
(3) Amos, A. T.; Burrows, B. L. *Adv. Quantum Chem.* **1973**, *7*, 289.
(4) Kosower, E. M. *J. Am. Chem. Soc.* **1958**, *80*, 3261.
(5) Mataga, N.; Kubota, T. *Molecular interactions and electronic spectra*; Dekker: New York, 1970.
(6) Kamlet, M. J.; Abbound, J.-L. M.; Abraham, M. H.; Taft, R. W. *J. Org. Chem.* **1983**, *48*, 2877.
(7) Reichardt, C. *Solvents and solvent effects in organic chemistry*; Wiley-VCH: Weinheim, Germany, 2003.
(8) Myers, A. B. *Ann. Rev. Phys. Chem.* **1998**, *49*, 267.
(9) Nicolet, P.; Laurence, C. *J. Chem. Soc. Perkin Trans.* **1986,** *2*, 1071.
(10) Rhodes, T. A.; Farid, S.; Goodman, J. L.; Gould, I. R.; Young, R. H. *J. Am. Chem. Soc.* **1999**, *121*, 5340.
(11) Bardeen, C. J.; Rosenthal, S. J.; Shank, C. V. *J. Phys. Chem. A.* **1999**, *103*, 10506.
(12) Myers, A. B.; Mathies, R. A. In *Biological Applications of Raman Spectroscopy*; Spiro, T. G., Ed.; Wiley: New York, 1987; Vol. 2, p 1.
(13) Kulinowski, K.; Gould, I. R.; Myers, A. B. *J. Phys. Chem.* **1995**, *99*, 9017.
(14) Myers, A. B. In *Laser Techniques in Chemistry*; Myers, A. B., Rizzo, T. R., Eds.; Wiley: New York, 1995; pp 325.
(15) Myers, A. B. *Chem. Rev.* **1996**, *96*, 911.
(16) Moran, A. M.; Delbecque, C.; Kelley, A. M. *J. Phys. Chem. A* **2001**, *105*, 10208.
(17) Moran, A. M.; Egolf, D. S.; Blanchard-Desce, M.; Kelley, A. M. *J. Chem. Phys.* **2002**, *116*, 2542.
(18) Woo, H. Y.; Liu, B.; Kohler, B.; Korystov, D.; Mikhailovsky, A.; Bazan, G. C. *J. Am. Chem. Soc.* **2005**, *127*, 14721.
(19) Zheng, L.; Jen, A. K.-Y. *Proc. SPIE* **2003**, *4797*, 163.
(20) Day, P. N.; Nguyen, K. A.; Pachter, R. *J. Chem. Phys.* **2006**, *125*, 094103.
(21) Song, Y.-Z.; Li, D.-M.; Song, X.-N.; Huang, X.-M.; Wang, C.-K. *THEOCHEM* **2006**, *772*, 75.
(22) Terenziani, F.; Morone, M.; Gmouh, S.; Blanchard-Desce, M. *ChemPhysChem.* **2006**, *7*, 685.
(23) Ray, P. C.; Leszczynski, J. *J. Phys. Chem. A* **2005**, *109*, 6689.
(24) Frediani, L.; Rinkevicius, Z.; Ågren, H. *J. Chem. Phys.* **2005**, *122*, 244104.
(25) Bartkowiak, W.; Zalesny, R.; Leszczynski, J. *Chem. Phys.* **2003**, *287*, 103.
(26) Zalesny, R.; Bartkowiak, W.; Styrcz, S.; Leszczynski, J. *J. Phys. Chem. A* **2002**, *106*, 4032.
(27) Luo, Y.; Norman, P.; Macak, P.; Ågren, H. *J. Phys. Chem. A* **2000**, *104*, 4718.
(28) Wang, C.-K.; Zhao, K.; Su, Y.; Ren, Y.; Zhao, X.; Luo, Y. *J. Chem. Phys.* **2003**, *119*, 1208.
(29) Wu, C.; Tretiak, S.; Chernyak, V. Y. *Chem. Phys. Lett.* Submitted.
(30) Barzoukas, M.; Muller, J.; Fort, A.; Marder, S. R.; Alain, V.; Blanchard-Desce, M. *Proc. SPIE* **1996**, *2852*, 132.
(31) Huyskens, F. L.; Huyskens, P. L.; Persoons, A. P. *J. Chem. Phys.* **1998**, *108*, 8161.
(32) Marder, S. R.; Beratan, D. N.; Cheng, L.-T. *Science* **1991**, *252*, 103.
(33) Wang, C.-K.; Wang, Y.-H.; Su, Y.; Luo, Y. *J. Chem. Phys.* **2003**, *119*, 4409.
(34) Willetts, A.; Rice, J. E. *J. Chem. Phys.* **1993**, *99*, 426.
(35) Woodford, J. N.; Pauley, M. A.; Wang, C. H. *J. Phys. Chem. A* **1997**, *101*, 1989.
(36) Yu, J.; Zerner, M. C. *J. Chem. Phys.* **1994**, *100*, 7487.
(37) Zuliani, P.; Del Zoppo, M.; Castiglioni, C.; Zerbi, G.; Marder, S. R.; Perry, J. W. *J. Chem. Phys.* **1995**, *103*, 9935.
(38) Fraga, E.; Loppnow, G. R. *J. Phys. Chem. B* **1998**, *102*, 7659.
(39) Kelley, A. M. *J. Phys. Chem. A* **1999**, *103*, 6891.
(40) McHale, J. L. *Acc. Chem. Res.* **2001**, *34*, 265.
(41) Biswas, N.; Umapathy, S. *J. Chem. Phys.* **2003**, *118*, 5526.
(42) Sension, R. J.; Kobayashi, T.; Strauss, H. L. *J. Chem. Phys.* **1987**, *87*, 6233.
(43) Foster, C. E.; Barham, B. P.; Reid, P. J. *J. Chem. Phys.* **2001**, *114*, 8492.
(44) Mayne, L. C.; Hudson, B. *J. Phys. Chem.* **1991**, *95*, 2962.
(45) Shoute, L. C. T.; Woo, H. Y.; Vak, D.; Bazan, G. C.; Kelley, A. M. *J. Chem. Phys.* **2006**, *125*, 054506.
(46) Helburn, R.; Ullah, N.; Mansour, G.; Maxka, J. *J. Phys. Org. Chem.* **1997**, *10*, 42.
(47) Oudar, J. L.; Chemla, D. S. *J. Chem. Phys.* **1977**, *66*, 2664.
(48) Teng, C. C.; Garito, A. F. *Phys. Rev. Lett.* **1983**, *50*, 350.
(49) Stähelin, M.; Burland, D. M.; Rice, J. E. *Chem. Phys. Lett.* **1992**, *191*, 245.
(50) Thomsen, C. L.; Thogersen, J.; Keiding, S. R. *J. Phys. Chem. A* **1998**, *102*, 1062.
(51) Kovalenko, S. A.; Schanz, R.; Farztdinov, V. M.; Hennig, H.; Ernsting, N. P. *Chem. Phys. Lett.* **2000**, *323*, 312.
(52) Moran, A. M.; Kelley, A. M. *J. Chem. Phys.* **2001**, *115*, 912.
(53) Kozich, V.; Werncke, W.; Dreyer, J.; Brzezinka, K.-W.; Rini, M.; Kummrow, A. *J. Chem. Phys.* **2002**, *117*, 719.
(54) An, Q.; Gilch, P. *Chem. Phys. Lett.* **2002**, *363*, 397.
(55) Faustino, W. M.; Petrov, D. V. *Chem. Phys. Lett.* **2002**, *365*, 170.
(56) Fujisawa, T.; Terazima, M.; Kimura, Y. *J. Chem. Phys.* **2006**, *124*, 184503.
(57) Shigeto, S.; Hiramatsu, H.; Hamaguchi, H.-o. *J. Phys. Chem. A* **2006**, *110*, 3738.
(58) Mansour, G.; Creedon, W.; Dorrestein, P. C.; Maxka, J.; MacDonald, J. C.; Helburn, R. *J. Org. Chem.* **2001**, *66*, 4050.
(59) Shoute, L. C. T.; Blanchard-Desce, M.; Kelley, A. M. *J. Phys. Chem. A* **2005**, *109*, 10503.
(60) Shoute, L. C. T.; Bartholomew, G. P.; Bazan, G. C.; Kelley, A. M. *J. Chem. Phys.* **2005**, *122*, 184508.
(61) Shoute, L. C. T.; Blanchard-Desce, M.; Kelley, A. M. *J. Chem. Phys.* **2004**, *121*, 7045.
(62) Schuddeboom, W.; Warman, J. M.; Biemans, H. A. M.; Meijer, E. W. *J. Phys. Chem.* **1996**, *100*, 12369.
(63) Frisch, M. J.; Trucks, G. W.; Schlegel, H. B.; Scuseria, G. E.; Robb, M. A.; Cheeseman, J. R.; Montgomery, Jr., J. A.; Vreven, T.; Kudin, K. N.; Burant, J. C.; Millam, J. M.; Iyengar, S. S.; Tomasi, J.; Barone, V.; Mennucci, B.; Cossi, M.; Scalmani, G.; Rega, N.; Petersson, G. A.; Nakatsuji, H.; Hada, M.; Ehara, M.; Toyota, K.; Fukuda, R.; Hasegawa, J.; Ishida, M.; Nakajima, T.; Honda, Y.; Kitao, O.; Nakai, H.; Klene, M.; Li, X.; Knox, J. E.; Hratchian, H. P.; Cross, J. B.; Bakken, V.; Adamo, C.; Jaramillo, J.; Gomperts, R.; Stratmann, R. E.; Yazyev, O.; Austin, A. J.; Cammi, R.; Pomelli, C.; Ochterski, J. W.; Ayala, P. Y.; Morokuma, K.; Voth, G. A.; Salvador, P.; Dannenberg, J. J.; Zakrzewski, V. G.; Dapprich, S.; Daniels, A. D.; Strain, M. C.; Farkas, O.; Malick, D. K.; Rabuck, A.

D.; Raghavachari, K.; Foresman, J. B.; Ortiz, J. V.; Cui, Q.; Baboul, A. G.; Clifford, S.; Cioslowski, J.; Stefanov, B. B.; Liu, G.; Liashenko, A.; Piskorz, P.; Komaromi, I.; Martin, R. L.; Fox, D. J.; Keith, T.; Al-Laham, M. A.; Peng, C. Y.; Nanayakkara, A.; Challacombe, M.; Gill, P. M. W.; Johnson, B.; Chen, W.; Wong, M. W.; Gonzalez, C.; Pople, J. A. *Gaussian 03*, revision C.02; Gaussian, Inc.: Wallingford, CT, 2004.

(64) Moran, A. M.; Bartholomew, G. P.; Bazan, G. C.; Kelley, A. M. *J. Phys. Chem. A* **2002**, *106*, 4928.

(65) Okamoto, H.; Tasumi, M. *Chem. Phys. Lett.* **1996**, *256*, 502.

(66) Li, B.; Johnson, A. E.; Mukamel, S.; Myers, A. B. *J. Am. Chem. Soc.* **1994**, *116*, 11039.

(67) Reichardt, C. *Chem. Rev.* **1994**, *94*, 2319.

(68) Chung, Y. C.; Ziegler, L. D. *J. Chem. Phys.* **1988**, *88*, 7287.

(69) Kelley, A. M.; Leng, W.; Blanchard-Desce, M. *J. Am. Chem. Soc.* **2003**, *125*, 10520.

(70) Kelley, A. M. *Int. J. Quantum Chem.* **2005**, *104*, 602.

(71) Barzoukas, M.; Runser, C.; Fort, A.; Blanchard-Desce, M. *Chem. Phys. Lett.* **1996**, *257*, 531.

(72) Lu, D.; Chen, G.; Perry, J. W.; Goddard, W. A., III. *J. Am. Chem. Soc.* **1994**, *116*, 10679.

(73) Thompson, W. H.; Blanchard-Desce, M.; Hynes, J. T. *J. Phys. Chem. A* **1998**, *102*, 7712.

(74) Maroncelli, M. *J. Chem. Phys.* **1991**, *94*, 2084.

(75) Zong, Y.; McHale, J. L. *J. Chem. Phys.* **1997**, *106*, 4963.